Photoreductive Self-Assembly from $[Mo^{VI}_7O_{24}]^{6-}$ to Anti-Tumoral $[H_2Mo^{V}_{12}O_{28}(OH)_{12}(Mo^{VI}O_3)_4]^{6-}$ in Aqueous Media

Toshihiro Yamase* and Eri Ishikawa

Chemical Resources Laboratory, Tokyo Institute of Technology,
R1-21 4259 Nagatsuta, Midori-ku, Yokohama 226-8503

CREST, Japan Science and Technology Agency (JST)

Received January 7, 2008; E-mail: tyamase@res.titech.ac.jp

The long-term photolysis of $[^{i}PrNH_3]_6[Mo_7O_{24}]\cdot 3H_2O$ in aqueous solutions at pH 5–6 is found to provide the formation of anti-tumoral $[H_2Mo^{V}_{12}O_{28}(OH)_{12}(Mo^{VI}O_3)_4]^{6-}$ species (**1a**), the core of which is a well-known ε-isomer ($\{\varepsilon$-$Mo^{V}_{12}\}$) of the Keggin anion showing edge-shared $Mo^{V}O_6$ octahedra in the arrangement of six diamagnetic Mo^{V}_2-pairs with a Mo^{V}–Mo^{V} bond distance of 2.6 Å. To obtain structural insight of **1a** in aqueous solutions from a viewpoint of the pharmaceutical mechanism, ^{95}Mo NMR, electronic absorption, IR, and electrospray ionization mass (ESI-MS) spectrometries of **1a** are investigated and indicate that the $\{\varepsilon$-$Mo^{V}_{12}\}$ core remains intact at pH 5–9 and that a detachment of the $Mo^{VI}O_3$ unit from **1a** proceeds at high pH level with an accompanying increase in the electronic transition of the Mo^{V}_2 pairs. Highly positive and negative potentials (0.8–0.9 and −1.1–−1.2 V) of oxidation and reduction current peaks for the Mo^{V}_2 pairs of **1a** assist the structural stability of the ε-Keggin $\{Mo^{V}_{12}\}$ framework in aerobic solutions. A plausible mechanism of the photoreductive self-assembly of $[Mo^{VI}_7O_{24}]^{6-}$ to **1a** through two- and four-electron reduction species, $[Mo^{V}_2Mo_5O_{22}(OH)_2]^{6-}$ ($\{Mo^{V}_2Mo^{VI}_5\}$) and $[Mo^{V}_4Mo_3O_{20}(OH)_4]^{6-}$ ($\{Mo^{V}_4Mo^{VI}_3\}$), is proposed in terms of the formation of a half molecule ($[HMo^{V}_6O_{18}(OH)_6(Mo^{VI}O_3)_2]^{11-}$) of **1a**, which is suggested by ESI-MS spectrometry of the photolytes.

Polyoxometalates (PMs) as discrete metal-oxide cluster anions, specified by high solubility in water and highly structure-selective pharmaceutical activity, have been investigated with an interest as a candidate of inorganic drugs.[1] In our study of in vivo inhibition of human-breast, -lung, and -colon cancer xenografts (MX-1, OAT, and CO-4, respectively) by a use of $[^{i}PrNH_3]_6[Mo_7O_{24}]\cdot 3H_2O$ (PM-8), the high cytotoxicity of the brown-colored photoreduced product (PM-17) has given us a mechanistic key that the antitumor activity of PM-8 is based on the formation of PM-17 through biological reductions in tumor cells.[2] The solution photolysis of PM-8 at pH 5–6 undergoes photoreductive condensations to yield the reddish-brown-colored PM-17 through the formation of a blue species. This blue species was identified as a diamagnetic two-electron-reduced species, $[(Mo^{VI}_6Mo^{V}O_{23})_2]^{10-}$ ($\{Mo_{14}\}$), which is a product through cis configurated dimeric condensation of the one-electron-reduced species of $[Mo^{VI}_6Mo^{V}O_{23}(OH)]^{6-}$.[3] Figure 1 shows the structural change of $[Mo^{VI}_7O_{24}]^{6-}$ (**i**) to $\{Mo_{14}\}$ as a result of the two-electron photoredox reaction with $[^{i}PrNH_3]^{+}$ at pH 5–6 (scheme 1).[4]

In the course of our structural investigation of PM-17 produced in the long-term photolysis of PM-8 at pH 5–6, we have recently determined the crystal structure of $[Me_3NH]_6$-$[H_2Mo^{V}_{12}O_{28}(OH)_{12}(Mo^{VI}O_3)_4]\cdot 2H_2O$ (**1**) as $[Me_3NH]^{+}$ salt of PM-17, the anion of which was the same for $[Me_2NH_2]_6$-$[H_2Mo^{V}_{12}O_{28}(OH)_{12}(Mo^{VI}O_3)_4]$ encountered in the reduction of $[NH_4]_6[Mo_7O_{24}]\cdot 4H_2O$ with hydrazinium dichloride in the presence of phenylphosphonic acid at 75 °C.[5] Figure 2 shows the structure (with atom labeling) and twelve intramolecular hydrogen bonds of **1a**, which were determined by the X-ray crystallographic analysis of **1**. Tables S1 and S2 list

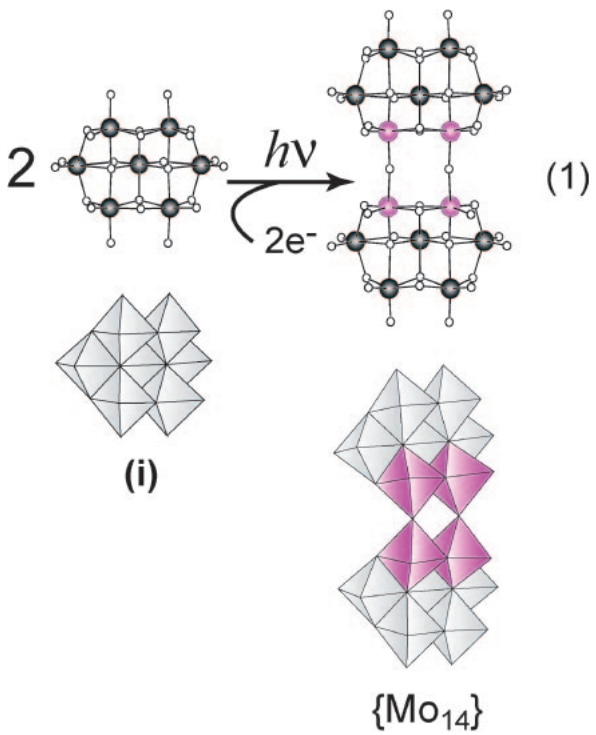

Figure 1. Structure change in the interconversion of $[Mo^{VI}_7O_{24}]^{6-}$ (**i**) to $[(Mo^{VI}_6Mo^{V}O_{23})_2]^{10-}$ ($\{Mo_{14}\}$) as a result of the two-electron photoredox reaction with $[^{i}PrNH_3]^{+}$ at pH 5–6 (scheme 1). Structures are shown by both atom and bond model and polyhedral model: Mo^{V} atoms and $Mo^{V}O_6$ octahedra are indicated by pink color. The d^1-electron injected into $\{Mo_{14}\}$ is delocalized within the almost linear (175°) Mo–O–Mo linkage in the center.

Published on the web August 11, 2008; doi:10.1246/bcsj.81.983

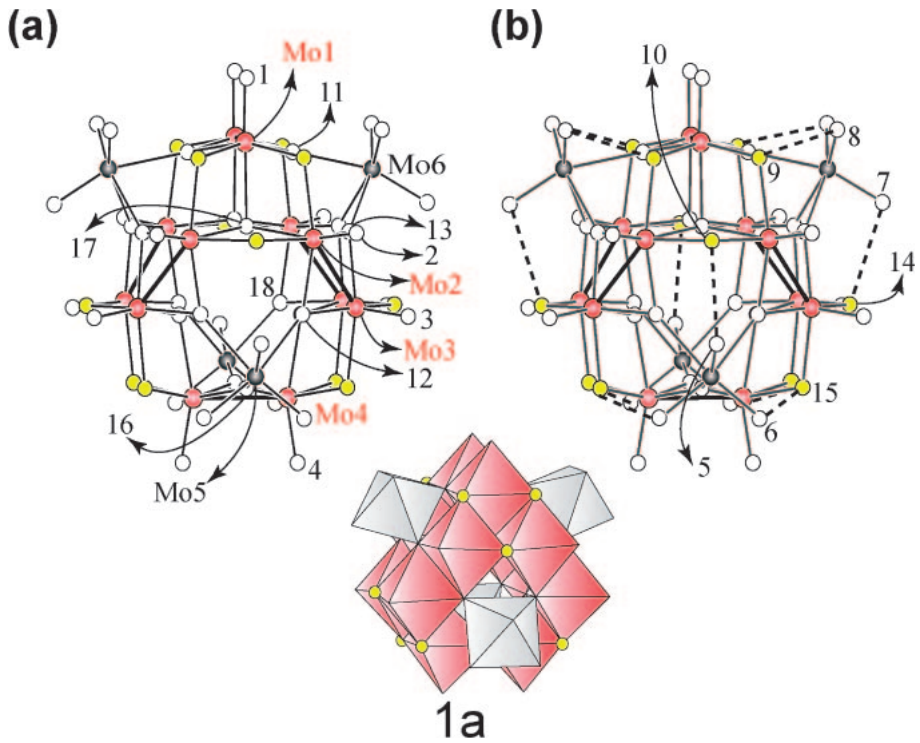

Figure 2. Structure of $[H_2Mo^{V}{}_{12}O_{28}(OH)_{12}(Mo^{VI}O_3)_4]^{6-}$ (**1a**) with the atom numbering scheme (a) and twelve plausible intramolecular hydrogen bonds indicated by dotted lines (b). Structures are shown by both atom and bond model and polyhedral model: Mo^{V}, Mo^{VI}, and μ_2-O atoms are indicated by red, gray, and yellow color, respectively.

the Mo–O bond distances and the inter-atomic distances of selected atoms, and the valence sum of the Mo–O bond strengths about given atoms, respectively. The core of the structure of **1a** is the ε-isomer ($\{\varepsilon$-$Mo^{V}{}_{12}\}$) of the Keggin anion, in which all $Mo^{V}O_6$ octahedra are linked by shared edges and arranged as six diamagnetic $Mo^{V}{}_2$-pairs with Mo^{V}–Mo^{V} bond distance of 2.6 Å. Each of the triangular faces of the truncated tetrahedral $\{\varepsilon$-$Mo^{V}{}_{12}\}$ cluster is capped by $Mo^{VI}O_3$. In **1a** the valence sum calculation (1.0–1.1) for twelve μ_2-O atoms (O9, O10, O14, and O15) identifies them as μ_2-hydroxo groups, which most likely form intramolecular hydrogen bonds with $Mo^{VI}O_3$ oxygen atoms (O5–O8) in corresponding O···O distances of 2.747(6)–2.824(9) Å. In addition, four μ_3-O atoms (O17 or O18) defining the tetrahedral cavity (in O···O distances of 3.34(1) Å) exhibit the valence sum of 1.3 (Table S2), suggesting that two protons are located on the four μ_3-O atoms in disorder. The same intramolecular hydrogen bonds and the disorder of two protons in the tetrahedral cavity were also pointed out previously.[5]

As was expected, **1** promisingly depressed the proliferation of human cancer cells such as AsPC-1 pancreatic and MKN-45 gastric cells.[6] This result let us to investigate the structural stability of **1** under physiological conditions. From the viewpoint of the pharmaceutical mechanism, we tried to characterize the structure of **1a** in aqueous solutions and to discuss the photochemical self-assembly processes from (**i**) to **1a**, with the help of crystal structure, spectrometries of IR, ^{95}Mo NMR, electronic absorption, and electrospray ionization mass (ESI-MS), and cyclic voltammograms. Interestingly, it is suggested that the detachment of $[Mo^{VI}{}_3O_{13}]^{8-}$ moieties, proposed in the photoreductive self-assembly of (**i**) to **1a**, leads to the formation of another Keggin (α-type) framework which was previously implied.[7]

Experimental

Preparation of $[Me_3NH]_6[H_2Mo^{V}{}_{12}O_{28}(OH)_{12}(Mo^{VI}O_3)_4]\cdot 2H_2O$ (1). $[^{i}PrNH_3]_6[Mo_7O_{24}]\cdot 3H_2O$ (PM-8) was synthesized according to a published procedure.[8] Reddish-brown crystals of $[Me_3NH]_6[H_2Mo^{V}{}_{12}O_{28}(OH)_{12}(Mo^{VI}O_3)_4]\cdot 2H_2O$ (**1**) were isolated from the solution of the prolonged photolysis of PM-8 at pH 5.4 or under subsequent alkalization by $^{i}PrNH_2$ (pH $\leq$ 12) as follows. An aqueous solution (20 mL) of PM-8 (0.3 g, 0.2 mmol) in a Pyrex tube was irradiated for 4 days using a 500-W super high-pressure mercury/xenon lamp. After $^{i}PrNH_2$ was added dropwise to the dark brown-colored photolyte to adjust the pH level to 8.8, $[Me_3NH]Cl$ (1 g, 10.4 mmol) was added and followed by cooling at 4 °C. Reddish-brown rod crystals were isolated after 1–2 weeks by filtration, successively washed by ice-cooled diethyl ether and cold water in the nitrogen gas atmosphere, and dried in a desiccator. Yield: 64.3 mg, 25.9% based on Mo, which corresponds to 46% for a hypothetical overall reaction "4(**i**) + 12e$^-$ → **1a** + $\{Mo^{VI}{}_{12}\}$" (vide infra). Calcd C, 7.78; H, 2.83; N, 3.03; Mo, 55.3%. Found: C, 7.58; H, 3.04; N, 3.44; Mo, 54.8%. Manganometric redox titration showed the presence of 11.6 ± 0.1 Mo^{V} centers in **1**. Together with the X-ray crystallographic analysis, the elemental analysis enables us to formulate **1** as given. The identity and purity of **1** were confirmed by IR, ^{95}Mo NMR, UV–vis, and ESI-MS spectra and cyclic voltammograms.

Instrumentation. IR (as KBr pellet) and UV–vis spectra were recorded on Jasco FT-IR 5000 and Jasco V-570 UV–vis–NIR spectrometers, respectively. The content of Mo was determined by inductively coupled plasma atomic emission spectroscopy

(ICP) on a Rigaku Spectro CIROS^{CCD} spectrometer.

The ^{95}Mo NMR data were obtained on a JEOL AL-300 NMR spectrometer equipped with a 10-mm molybdenum probe (19.6 MHz). Preaquisition delay of 400 μs was used to reduce the effect of probe ringing. Spectra of 4.5–4.6 mM **1** in D_2O were recorded at 22 °C unless specified otherwise, and 2 M Na_2MoO_4 in D_2O was used as external standard.

Cyclic voltammograms were measured with a combination of a potentiostat (Hokuto Denko HA-301) with a function generator (Nikko Keisoku NFG-3). Aqueous solutions (of 5–10 mL) containing 0.2 mM **1** and 0.1 M $NaClO_4$ were purged with nitrogen gas for 10 min and measured with a scan rate of 100 mV s^{-1} by using a glassy carbon ($\phi = 1$ mm) working electrode, a Pt-wire counter electrode, and a Ag/AgCl reference electrode. The scan rate dependence of the cyclic voltammograms was done in the range of 10–400 mV s^{-1}. After each measurement, the working electrode was polished with 0.3-μm Al_2O_3 and rinsed with water to ensure reproducible results.

The mass spectra were recorded by using an ion trap mass spectrometer (Bruker Daltonics microTOF) equipped with an electrospray ionization (ESI) source operated in negative-ion mode. The tip of the capillary and the capillary exit were maintained at potentials of 3.5–3.8 kV and −33 V respectively, relative to the ground. The source temperature was 120 °C. Sample solutions (1.0 mM based on PM-8 in water) were infused by using a syringe pump into the ESI source at a flow rate of 180 μL h^{-1}. An analysis required a careful tuning of the electrospray source for obtaining a global view of intact polyoxomolybdates together with few characteristic fragments. In particular, the voltage difference ($\Delta U_{CE\text{-}Sk}$) between the orifice and the first skimmer has to be set such to avoid decomposition of the anion in the ion source. As a result, attribution of the observed signals to complex stoichiometries was formulated readily, and the spectra reflected the solution composition. Typically a low declustering potential $\{\Delta U_{CE\text{-}Sk} = -5\,V = -33 - (-28)\,V\}$ was used to keep the complexes intact. When high potentials, $\Delta U_{CE\text{-}Sk} = -40\,V = -80 - (-40)\,V$ for example, resulted in strong asymmetric distribution patterns of signals due to in-source fragmentation.

Crystal Data for 1. $H_{78}Mo_{16}N_6O_{54}C_{18}$, MW: 2777.86, Space group: *Cmcm* (No. 63), $a = 17.838(5)$, $b = 20.663(6)$, $c = 20.325(6)$ Å, $Z = 4$, $V = 7491(5)$ Å^3, $\rho = 2.46$ g cm^{-3}, $\mu = 26.72$ cm^{-1}, $F(000) = 5328$. Crystal size: $0.4 \times 0.4 \times 0.2$ mm^3. Crystal was coated with paraffin oil and mounted in a loop. Intensity data were measured on a Rigaku/MSC Saturn CCD diffractometer with graphite monochromatized Mo Kα radiation (=0.71071 Å) at 173 K. Data collection proceeded by using ω-scan at 0.5° scan and $\chi = 45°$ in two runs (with 360 frames respectively) of $-110.0° < \omega < 70.0°$, $\phi = 0°$; $-110.0° < \omega < 70.0°$, $\phi = 90°$. The crystal-to-detector distance was 45.1 mm. The exposure rate was 5 s/°. The detector swing angle was 20.06°. A total of 58270 reflections ($2.2° < \theta < 27.5°$) was collected of which 4554 unique reflections ($R_{int} = 0.034$) were used. Transmission factors were 0.30–0.59. The structure was solved by a direct method (SHELXS-97) and refined based on 4322 observed reflections with $I > 2\sigma(I)$ and 225 parameters to $R_1 = 0.046$ and $R_w = 0.121$ (refined against $|F^2|$). For all the unique reflections $R_1 = 0.050$ and $R_w = 0.122$ were obtained. The highest residual electron density was 2.23 eÅ^{-3} at 1.53 Å from O20 atom. Lorentz polarization factor was applied and a numerical absorption correction (multi-scan) using equivalent reflections was performed with the program (numerical; T. Higashi, *Program for Absorption Correction*, Rigaku Corporation, Tokyo, **1999**). All the Mo and O atoms for the anion were refined anisotropically, and all the C, O (for water), and N atoms isotropically. Site occupancies of C, N, and O atoms for cations and lattice-water molecules except for C4 were set to be 1/2 through the refinement of their thermal parameters. Tables S1 and S2 list the Mo–O bond distances and the inter-atomic distances of selected atoms, and the valence sum of the Mo–O bond strengths about given atoms, respectively. Further details on the crystal structure investigations may be obtained from Cambridge Crystallographic Data Center (CCDC), e-mail: deposit@ccdc.cam.ac.uk, on quoting the depository numbers CCDC-626588 $[Me_3NH]_6[H_2Mo^{V}_{12}O_{28}(OH)_{12}(Mo^{VI}O_3)_4]\cdot 2H_2O$ (**1**).

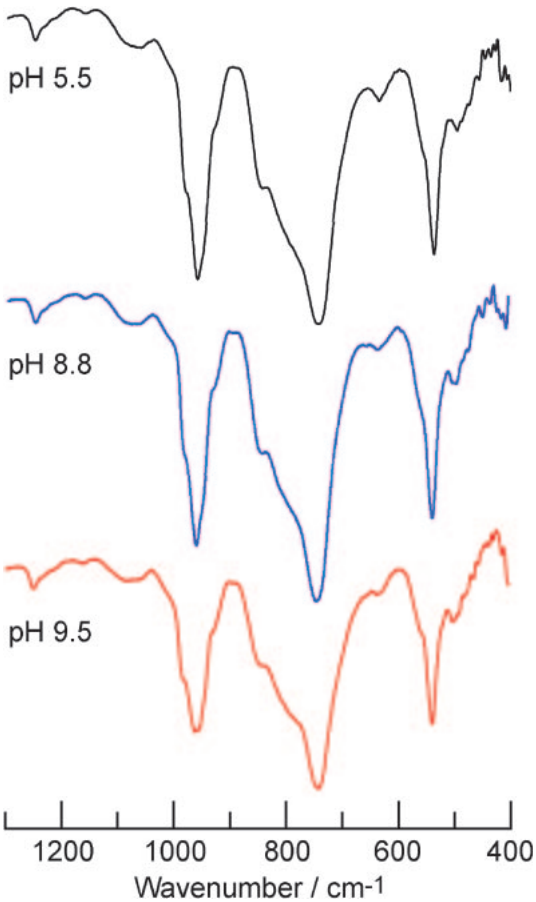

Figure 3. FT-IR spectra of crystalline of **1** isolated at three pH levels of 5.5, 8.8, and 9.5.

Results and Discussion

Structural Characterization of 1a in Aqueous Solutions. Figure 3 shows IR spectra of crystals (for **1**) isolated at three different pH levels of 5.5, 8.8, and 9.5. All the spectral patterns exhibiting terminal Mo–O stretching and Mo–O–Mo bridging frequencies at 400–1300 cm^{-1} are quite similar, suggesting that the ε-Keggin $\{Mo^{V}_{12}\}$ core capped by four $Mo^{VI}O_3$ units is common to the crystals isolated at pH levels of 5–9.

Figure 4 shows ^{95}Mo NMR spectra of **1** in anaerobic D_2O at three different pD levels of 5.4, 6.9, and 9.2. **1** showed a resonance peak with broad half-widths of 70–80 Hz around δ 304 due to four $Mo^{VI}O_3$ units, in contrast to ^{95}Mo NMR-inactive $[PMo^{V}_8Mo^{VI}_4O_{36}(OH)_4\{La(H_2O)_4\}_4]^{5+}$,[9] the structure of which shows that the crystallographic disorder or valence elec-

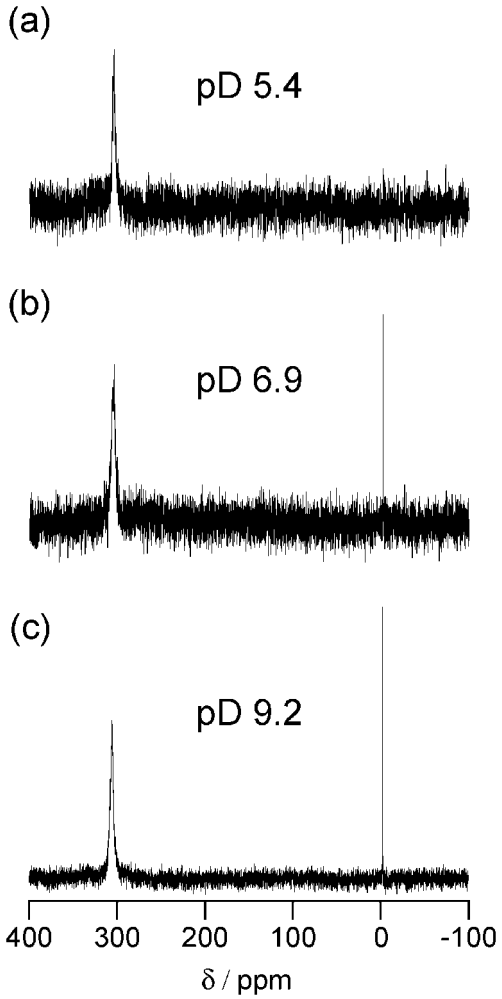

Figure 4. ^{95}Mo NMR spectra of **1** in anaerobic D_2O at three pD levels of 5.4, 6.9, and 9.2.

tron delocalization equalizes the arrangements of four Mo^{VI} atoms in the ε-Keggin core capped by four $\{La(H_2O)_4\}$ groups.[10] A weak intensity line (less than 5% relative to the δ 304 line) with narrow half-widths of 2 Hz around δ −2.0, which appears at high pD levels (≥6.9), is likely to be assigned to the hydrated octahedral derivative of the $Mo^{VI}O_3$ unit detached from **1a**. The detachment of a capping unit has also been pointed for $[PMo^{V}_{8}Mo^{VI}_{4}O_{36}(OH)_4\{La(H_2O)_4\}_4]^{5+}$ where the ε-Keggin ion is involved in an equilibrium with La^{3+} ions, as implied by the ^{31}P NMR spectrometry.[10]

Figure 5 shows UV–vis absorption spectra of **1** at pH levels of 5.4, 6.9, and 9.2. The reddish-brown color (as reflected by $\varepsilon_{380} = 2.3 \times 10^3$ and $3.3 \times 10^3\,cm^{-1}\,M^{-1}$ at pH 5.4 and 9.2 respectively, for example) is attributed to the electronic transition of $\{(d_{xy}{}^{A} + d_{xy}{}^{B})/\sqrt{2}\} \rightarrow \{(d_{xy}{}^{A} - d_{xy}^{B})/\sqrt{2}\}$ for the localized Mo^{V}_{A}–Mo^{V}_{B} pairs rather than the intervalence $Mo^{V} \rightarrow Mo^{VI}$ charge-transfer band. An increase in the absorption coefficient with alkalinity may be associated with partial breakage of the intramolecular hydrogen bonds, which would reduce distortion of the $Mo^{V}O_6$ octahedra and possibly lead to detachment of the $Mo^{VI}O_3$ unit (Figure 4),[11] since all the twelve $Mo^{V}O_6$ μ_3-oxygen atoms (O11–13 and O16) coordinating the $Mo^{VI}O_3$ unit showed asymmetric distances of

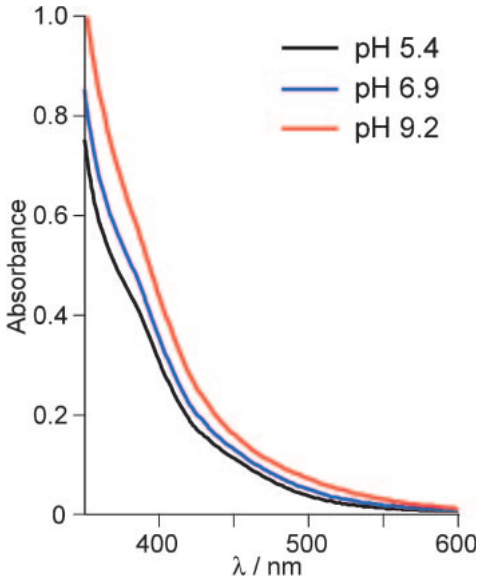

Figure 5. UV–vis absorption spectra of **1** (0.2 mM) at pH levels of 5.4, 6.9, and 9.2.

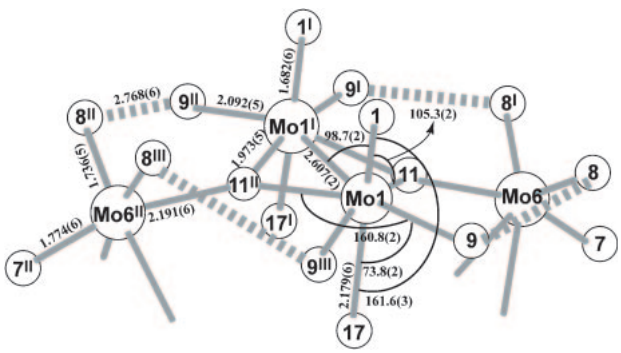

Figure 6. Coordination environment of the diamagnetic Mo^{V}_2 pair at Mo(1) sites of **1**. Distances and angles are in Å and °, respectively. Superscript on atoms number indicates each symmetry code: **I** $-x$, y, z; **II** $-x$, y, $3/2 - z$; **III** x, y, $3/2 - z$.

Mo^{V}–O (1.960(4)–1.974(4) Å) and Mo^{VI}–O (2.190(6)–2.259(5) Å) at the Mo^{V}–O–Mo^{VI} linkage in the crystal structure (Table S1). Figure 6 exemplifies the coordination environment of the diamagnetic Mo^{V}_2 pair at Mo(1) sites, where each $Mo^{V}O_6$ octahedron is highly distorted.

Figure 7 shows cyclic voltammograms of **1** on the glassy carbon electrode in anaerobic aqueous solutions (at pH 5–9) containing 0.1 M $NaClO_4$. As shown in Figure 7a, the first cycle toward the positive potential gives an irreversible oxidation peak around 0.8 V (at the threshold of 0.3 V) vs. Ag/AgCl reference electrode at the scan rate of 100 mV s^{-1}. Since the oxygen molecule showed an irreversible reduction current peak at much more negative potential (Figure S1) around −0.6 V (at the threshold of −0.3 V) at the same scan rate, it is unlikely that the oxidative decomposition (of the Mo^{V}_2 pairs) of **1a** at pH 5–9 occurs with an involvement of oxygen molecules. The first cycle toward the negative potential in the anaerobic system at a scan rate of 100 mV s^{-1} gives asymmetric reduction and oxidation peaks around at −1.2 and −1.0 V at three

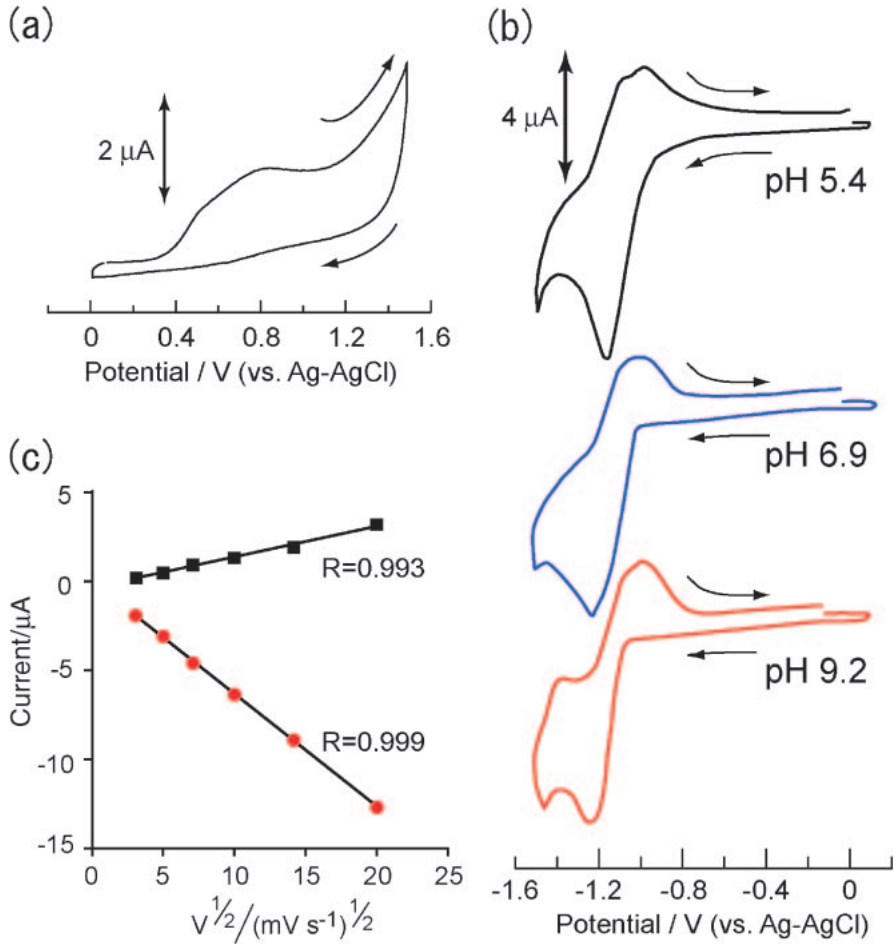

Figure 7. Cyclic voltammograms (a and b) of **1** (0.2 mM) with a scan rate of 100 mV s^{-1} on a glassy carbon electrode in aqueous solutions (at pH 5.4, 6.9, and 9.2) containing 0.1 M $NaClO_4$ under anaerobic conditions. Relationships (c) between peak currents and scan rates, taking the $Mo^{V}{}_2$-pair oxidation (black filled square) and reduction (red filled circle) peak at 0.8–0.9 and −1.1–−1.2 V as representatives.

different pH levels of 5.4, 6.9, and 9.2 (Figure 7b), indicating an irreversible reduction process. The peak currents for oxidation (around at 0.8–0.9 V) and reduction (around at −1.1–−1.2 V) showed a shift of the peak potential to positive and negative potential respectively with increasing the scan rate in the range 10–400 mV s^{-1}, and were approximately linearly proportional to the square root of scan rates (Figure 7c). The difference between the oxidation and reduction peak potentials (0.8 and −1.2 V, respectively at 100 mV s^{-1} for example) for the first cycle is close to the energy (2.1 eV) of the electronic absorption threshold (around at 600 nm) of **1** (Figure 5). The irreversibility of the electrochemical reduction in the first cycle toward the negative potential reveals the antibonding character of the LUMO ($(d_{xy}{}^{A} - d_{xy}{}^{B})/\sqrt{2}$) for the diamagnetic $Mo^{V}{}_{A}$–$Mo^{V}{}_{B}$ bond, which implies the reductive cleavage of the Mo^{V}–Mo^{V} bond. The highly positive and negative potentials of oxidation and reduction current peaks for the $Mo^{V}{}_2$ pairs of **1a** assist the structural stability of the ε-Keggin $\{Mo^{V}{}_{12}\}$ framework in aerobic solutions at pH 5–9, although the equilibrium involving the detachment of $Mo^{VI}O_3$ unit from **1a** exists (Figure 4).

Figure 8 shows the ESI-MS spectrum recorded in negative ion mode of a 5×10^{-4} M solution of **1** in water. There was no observable oxidation of **1a** by dissolved oxygen during ESI-MS measurements, as supported by the cyclic voltammograms of **1** (Figure 7 and Figure S1). The 1:4 complex consisting of one $\{\varepsilon\text{-}Mo^{V}{}_{12}\}$ and four $Mo^{VI}O_3$ units is detected as $[H_2Mo^{V}{}_{12}O_{28}(OH)_{12}(Mo^{VI}O_3)_4]^{6-}$ with the required number of H^+ cations to obtain a charge state distribution from 4− to 2−. The base peak at $m/z = 794.2$ features a triple-charge signature with an isotropic separation of ca. 0.33 m/z units. Other diagnostic ion peaks are found at $m/z = 595.4$ and 1192.8, and display the isotropic envelope spaced by ca. 0.25 and 0.50 m/z units, i.e. two different charge states 4− and 2−. Theoretical simulation of the three observed isotropic patterns allows the assignment of the pertinent molecular formula, $[H_3\{H_2Mo^{V}{}_{12}O_{28}(OH)_{12}(Mo^{VI}O_3)_4\}]^{3-}$, $[H_2\{H_2Mo^{V}{}_{12}O_{28}(OH)_{12}(Mo^{VI}O_3)_4\}]^{4-}$, and $[H_4\{H_2Mo^{V}{}_{12}O_{28}(OH)_{12}(Mo^{VI}O_3)_4\}]^{2-}$, with the highest peak of the calculated isotopic distributions located at $m/z = 794.9$, 595.9, and 1192.9, respectively. Detachment of one $Mo^{VI}O_3$ unit from **1a** accounts for the presence of other minor peaks at $m/z =$ 746.2 and 1120.5, ascribable to the 3− species and the 2− species which were derived from the 1:3 complex of $[H_2Mo^{V}{}_{12}O_{28}(OH)_{12}(Mo^{VI}O_3)_3]^{6-}$, $[H_3\{H_2Mo^{V}{}_{12}O_{28}(OH)_{12}(Mo^{VI}O_3)_3\}]^{3-}$ ($m/z = 746.9$), and $[H_4\{H_2Mo^{V}{}_{12}O_{28}$-

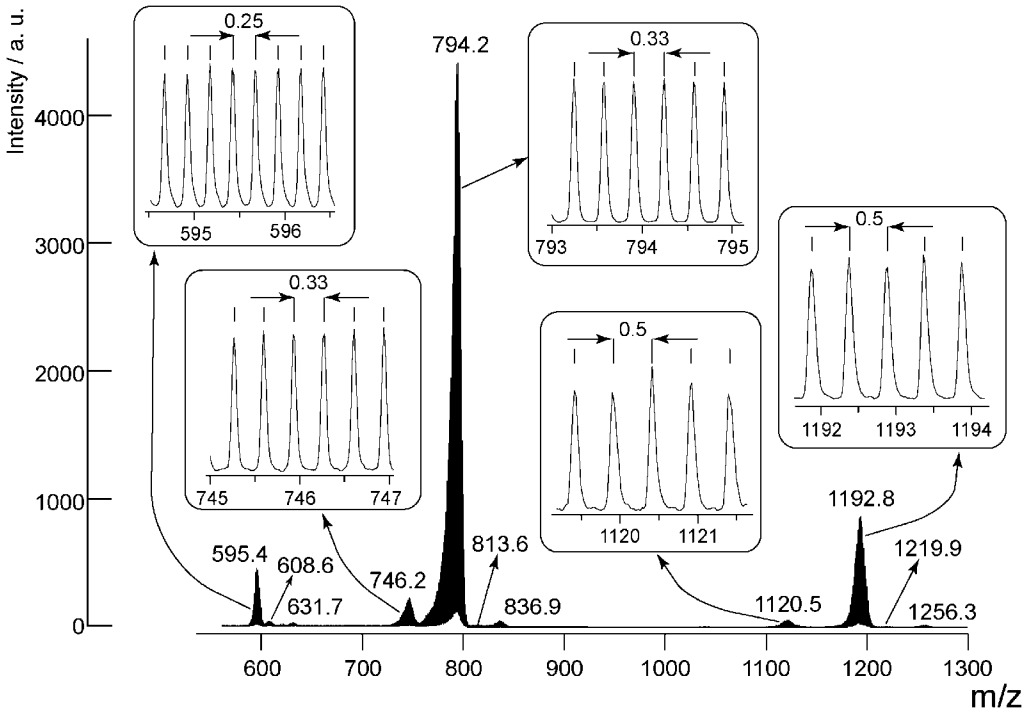

Figure 8. ESI-MS spectrum recorded in negative ion mode of a 5×10^{-4} M solution (at pH 5.4) of **1** in water. Insets are expansions of signals.

$(OH)_{12}(Mo^{VI}O_3)_3\}]^{2-}$ ($m/z = 1120.9$), respectively. Two and three sets of multiply charged ions with very weak intensity around at $m/z = 836.9$ and 1256.3, and 608.6, 813.6, and 1219.9 corresponding to two and three different charge states 3− and 2−, and 4−, 3−, and 2−, may be identified to the solvate molecules $[(H_2O)_7H_3\{H_2Mo^{V}{}_{12}O_{28}(OH)_{12}(Mo^{VI}O_3)_4\}]^{3-}$ and $[(H_2O)_7H_4\{H_2Mo^{V}{}_{12}O_{28}(OH)_{12}(Mo^{VI}O_3)_4\}]^{2-}$, and $[(H_2O)_3H_2\{H_2Mo^{V}{}_{12}O_{28}(OH)_{12}(Mo^{VI}O_3)_4\}]^{4-}$, $[(H_2O)_3H_3\{H_2Mo^{V}{}_{12}O_{28}(OH)_{12}(Mo^{VI}O_3)_4\}]^{3-}$, and $[(H_2O)_3H_4\{H_2Mo^{V}{}_{12}O_{28}(OH)_{12}(Mo^{VI}O_3)_4\}]^{2-}$, which are expected at $m/z = 836.9$ and 1255.9, and 609.5, 812.9, and 1219.9, respectively. To further test the detachment of $Mo^{VI}O_3$ units from **1a**, **1** was dissolved in a $^{i}PrNH_2$-adjusted alkaline solution at pH 11.4 and mass spectra were recorded under the same experimental conditions. Figure 9 shows the spectrum of **1** at pH 11.4. In addition to the 1:3-complex-derived peak at $m/z = 746.9$, two 1:2-complex-derived peaks at $m/z = 699.0$ and 1048.5, which were assigned to $[H_3\{H_2Mo^{V}{}_{12}O_{28}(OH)_{12}(Mo^{VI}O_3)_2\}]^{3-}$ ($m/z = 699.0$) and $[H_4\{H_2Mo^{V}{}_{12}O_{28}(OH)_{12}(Mo^{VI}O_3)_2\}]^{2-}$ ($m/z = 1048.9$) respectively, were developed with an accompanying decrease in parent peak (due to the 1:4 complex) at $m/z = 794.2$. This result implies that the alkalization of the aqueous solution containing 1:4 complex has a significant effect on the detachment of $Mo^{VI}O_3$ units which progressively yield 1:3 complex and MoO_6-octahedral derivative, in agreement with the results of ^{95}Mo NMR spectrometry (Figure 4), probably according to the equilibrium reaction of "$[(1:4)\text{-}\mathbf{1a}]^{6-} + OH^- + 2H_2O \leftrightarrow [1{:}3\ \text{complex}]^{7-} + [Mo^{VI}O_2(H_2O)_2(OH)_2]$." Thus, the detachment of $Mo^{VI}O_3$ units from **1a** is strongly associated with the breakage of intramolecular hydrogen bonds (Figure 2) with a resultant increase in the electronic transition moment of the $Mo^{V}{}_2$ pair (Figures 5 and 6).

Photoreductive Self-Assembly from $[Mo_7O_{24}]^{6-}$ to 1a. Since the photoreduction of the $[Mo_7O_{24}]^{6-}$ lattice proceeds through transfer of the hydrogen-bonded proton of the electron donor to the $Mo^{VI}O_6$-oxygen atom to yield a $Mo^{V}O_5(OH)$ site,[11] it is implied that the formation of **1a** lattice incorporating 12 hydroxo groups in aqueous solutions results from the multi-electron reduction of $[Mo_7O_{24}]^{6-}$. $\{Mo_{14}\}$ isolated in the short-term steady-state photolysis of (**i**) was a two-electron reduction species, in which the two electrons were delocalized within two sets of two MoO_6 octahedra linked through an axial μ_2-oxo oxygen atom with the Mo–O–Mo bond-angle of 175° in the center (Figure 1).[3] Thus, a C_{2v}-symmetric geometry of (**i**) lets us assume that the photoreduction of (**i**) in solutions occurs equally at the two MoO_6 octahedra forward in line at the central horizontal level above or below, to yield two-electron-reduced $\{Mo_7\}$ species (**ii**) (scheme 2 in Figure 10). On the other hand, the solid-state photochemistry of alkylammonium heptamolybdates such as PM-8 ($[^{i}PrNH_3]_6[Mo_7O_{24}]\cdot 3H_2O$) and $[PrNH_3]_6[Mo_7O_{24}]\cdot 3H_2O$ showed the formation of $Mo^{V}O_5(OH)$ at either end of three MoO_6 octahedra at the central horizontal level.[12,13] This suggests that the photoreduction of (**i**) in solutions occurs also equally at both ends at the central horizontal level of three MoO_6 octahedra, to yield another two-electron-reduced $\{Mo_7\}$ species (**iii**) (scheme 3 in Figure 10).[12b] Figure 10 shows that the prolonged photolysis of PM-8 at pH 5–6 starts with the formation of two types of two-electron reduction intermediates, (**ii**) and (**iii**), which is coupled with the oxidation of $[^{i}PrNH_3]^+$ as a two proton/electron donor.[4]

The change of framework from (**ii**) and (**iii**) anions to **1a** let us propose five pathways in the (**i**) → **1a** self-assembly, as schematized by polyhedral model in Figure 11: 1) formation of four-electron-reduced $\{Mo_7\}$ species (**iv**), probably formu-

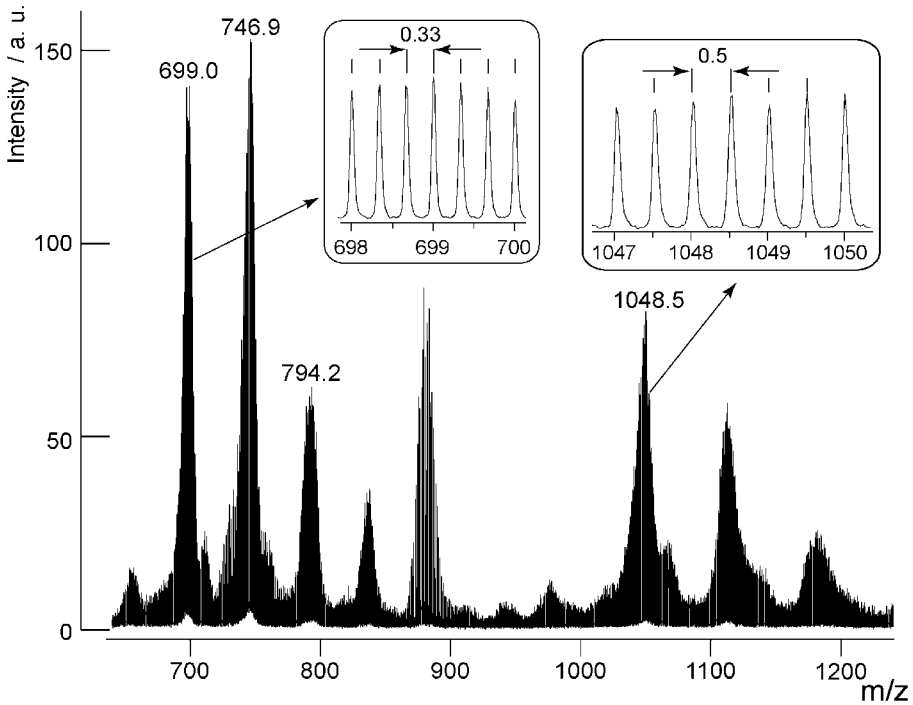

Figure 9. ESI-MS spectrum recorded in negative ion mode of a 5×10^{-4} M solution of **1** at pH 11.4. Insets are expansions of signals.

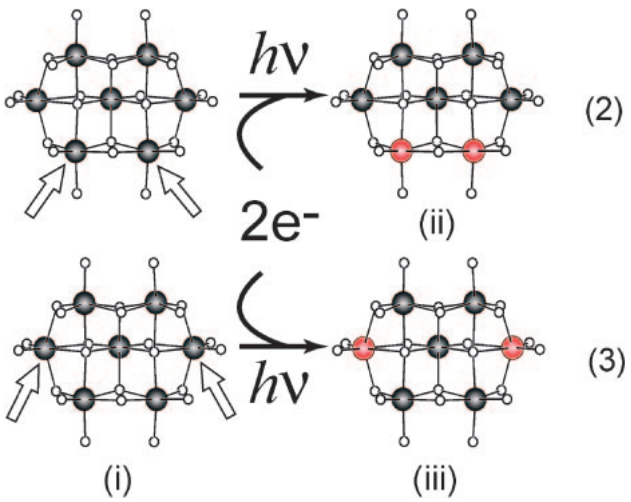

Figure 10. Schematic two pathways for the formation of two-electron reduction species of $[Mo^{V}_{2}Mo^{VI}_{5}O_{22}(OH)_{2}]^{6-}$ (schemes 2 and 3) at the beginning of prolonged photolysis of PM-8 in solutions at pH 5–6. Light arrows indicate photoreducible MoO_6 octahedral sites, and Mo^{V} and Mo^{VI} atoms are indicated by red and gray color, respectively.

lated by $[Mo^{V}_{4}Mo^{VI}_{3}O_{20}(OH)_{4}]^{6-}$, as a result of the reduction at the same sites as for (**ii**) and (**iii**) (scheme 4 in Figure 11), 2) subsequent condensation of two $\{Mo^{V}O_5(OH)\}$ octahedra (produced during liberation of one $\{Mo^{VI}_{3}\}$ and two $\{Mo^{VI}_{1}\}$ units from (**iii**)) at the two ends at the central horizontal level in (**iv**), to yield the two Mo^{V}_{3}-triads containing six-electron reduction $\{Mo^{V}_{6}Mo^{VI}_{3}\}$ intermediate (**v**) (scheme 5 in Figure 11), where $\{Mo^{VI}_{3}\}$, $\{Mo^{VI}_{1}\}$, and $\{Mo^{V}_{6}Mo^{VI}_{3}\}$ are temporarily formulated by $[Mo^{VI}_{3}O_{13}]^{8-}$, $[Mo^{VI}O_2$-

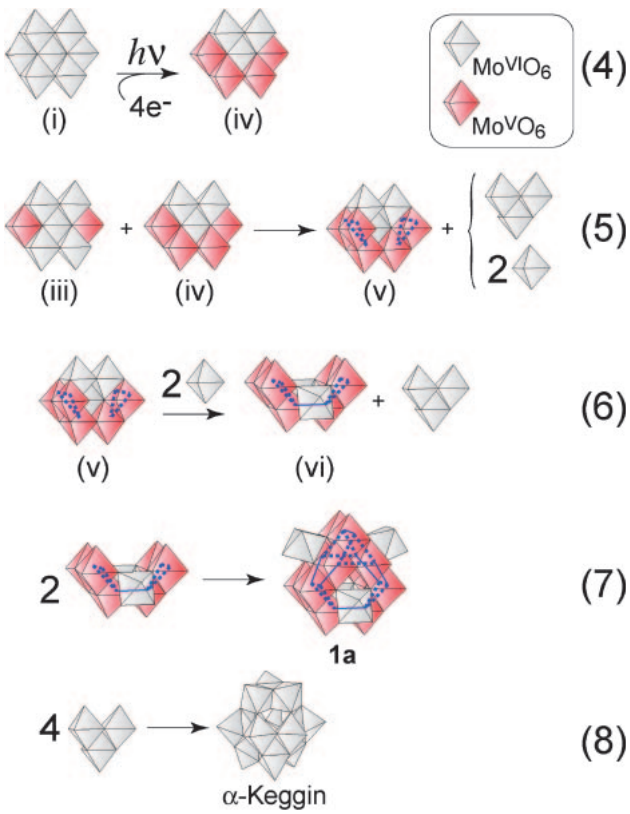

Figure 11. Schematic pathways for (**i**) → **1a** through four-electron reduction in the prolonged photolysis of PM-8 in solutions at pH 5–6. Red and gray color by the polyhedral model indicates $Mo^{V}O_6$ and $Mo^{VI}O_6$ octahedron sites, respectively. Blue solid and dotted lines indicate Mo^{V}–Mo^{V} bond (with 2.6-Å bond distance) and Mo^{V}_{3} triad, respectively.

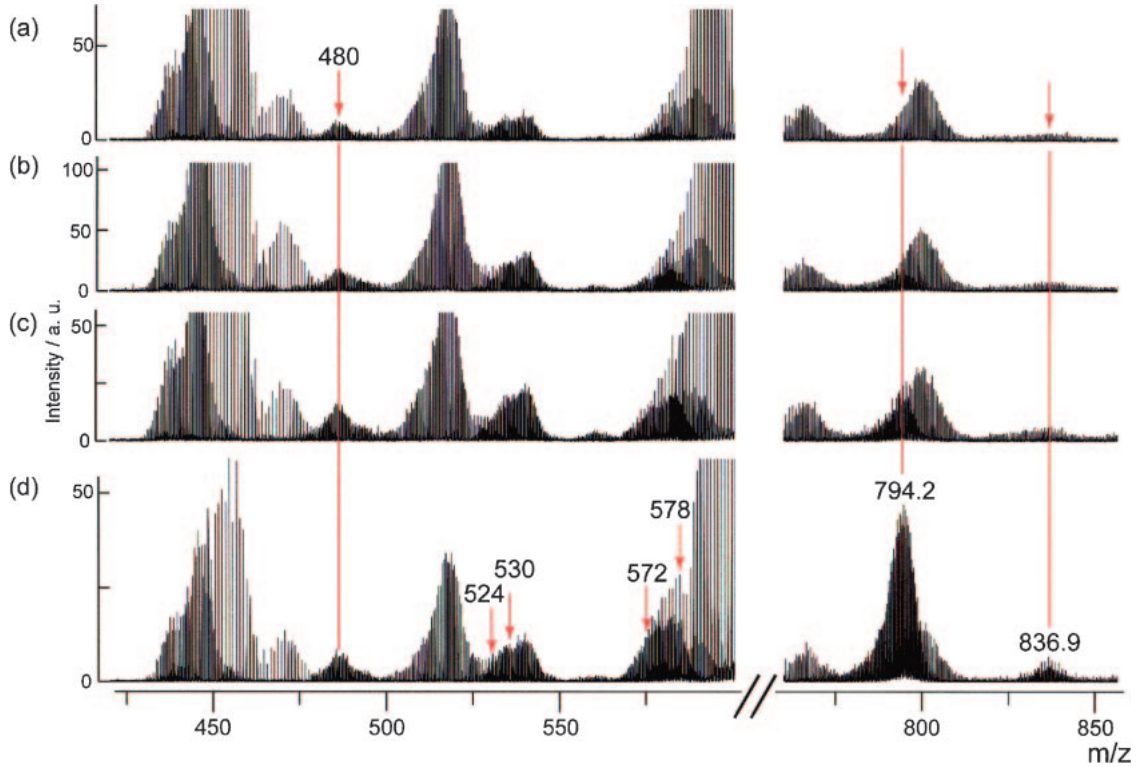

Figure 12. ESI-MS spectra of 10-fold diluted samples (by water) for 3-, 6-, 10-, and 24-h photolyses (a–d, respectively) of PM-8 at pH 5.5.

$(H_2O)_2(OH)_2]$, and $[Mo^V_6Mo^{VI}_3O_{22}(OH)_6]^{2-}$ respectively: the latter corresponds to a mono-lacunary species of $[V^V_{10}O_{28}]^{6-}$ or $[Nb^V_{10}O_{28}]^{6-}$ containing all the penta-valent metal (same as Mo^V),[14,15] 3) formation of the Mo^V–Mo^V bond between Mo^V_3 triads of the prism-like Mo^V_6 moiety with a removal of $\{Mo^{VI}_3\}$, which is assisted by condensation with two $\{Mo^{VI}_1\}$, to yield $\{Mo^V_6Mo^{VI}_2\}$ (**vi**) (temporarily formulated by $[HMo^V_6O_{18}(OH)_6(Mo^{VI}O_3)_2]\}^{11-}$) as a half molecule of **1a** (scheme 6 in Figure 11), 4) S_4-symmetric condensation of two (**vi**) with additional formation of four Mo^V–Mo^V bonds, to yield **1a** (scheme 7 in Figure 11). Schemes 4–7 proposed for the (**i**) → **1a** self-assembly indicates a possibility of the construction of α-Keggin type $\{Mo^{VI}_{12}\}$ through the aggregation of four remaining $\{Mo^{VI}_3\}$ of three edge-shared MoO_6 octahedra (scheme 8 in Figure 11), as implied previously for the photolysis of PM-8 at pH 5–6:[7] thus, an overall reaction may be given by "4 (**i**) + $12e^-$ → **1a** + $\{Mo^{VI}_{12}\}$" (where $12e^-$ originate from six $[^iPrNH_3]^+$ cations as two-electron donors.[4]) The Mo^V–Mo^V bonds (with $(d_{xy}{}^A + d_{xy}{}^B)/\sqrt{2}$, HOMO) for each Mo^V_3 triad in (**v**) is frustrated among three edge-shared $Mo^VO_5(OH)$ octahedra and therefore the formation of the diamagnetic Mo^V_2 pairs in **1a** seems to be rationalized by the condensation of two $\{Mo^{VI}_1\}$ units between the Mo^V_3 triads.

ESI-MS spectra of the photolytes (diluted 10-fold by water) at several stages of the photolysis have been measured for the detection of the intermediates involved in the photolysis. Figure 12 shows ESI-MS spectra acquired for 3-, 6-, 10-, and 24-h photolyses. The corresponding spectra at 0- and 48-h (as before and full photolysis) are shown in Figure S2. A peak with charged state 3− around at $m/z = 480$ is observed for the photolysis, which is possibly explained by $\{(Me_3NH)_3H_5[HMo^V_6O_{18}(OH)_6(Mo^{VI}O_3)_2]\}^{3-}$ ($m/z = 480.2$) or $\{(H_2O)_{10}H_8[HMo^V_6O_{18}(OH)_6(Mo^{VI}O_3)_2]\}^{3-}$ ($m/z = 481.2$) as a $[Me_3NH]^+$-attached or solvate species of a half molecule of **1a** (**vi**). Since two peaks with charged state 3− at $m/z =$ 794.2 and 836.9, observed for 24-h photolysis (Figure 12d) would be assigned to $[H_3\{H_2Mo^V_{12}O_{28}(OH)_{12}(Mo^{VI}O_3)_4\}]^{3-}$ and $[(H_2O)_7H_3\{H_2Mo^V_{12}O_{28}(OH)_{12}(Mo^{VI}O_3)_4\}]^{3-}$ respectively (Figure 8), the formation of **1a** occurs within 24-h photolysis. Four other dominant peaks (around at $m/z = 524$, 530, 572, and 578) consisting of two sets of two species at intervals of about 6 with charged state 3− are observed (Figures 12b–12d), which may be assigned to the solvated lacunary species derived from both ε-Keggin $[Mo^V_{12}O_{28}(OH)_{12}]^{8-}$ and 1:1 complex: $\{(H_2O)H_9[Mo^V_{10}O_{26}(OH)_{10}]\}^{3-}$ ($m/z = 524.2$), $\{(H_2O)_2H_9[Mo^V_{10}O_{26}(OH)_{10}]\}^{3-}$ ($m/z = 530.2$), $\{(H_2O)H_9[Mo^V_{10}O_{26}(OH)_{10}(Mo^{VI}O_3)]\}^{3-}$ ($m/z = 572.1$), and $\{(H_2O)_2H_9[Mo^V_{10}O_{26}(OH)_{10}(Mo^{VI}O_3)]\}^{3-}$ ($m/z = 578.1$) respectively. The possibility that these lacunary species result from the evaporation process in the ESI-MS technique is not excluded. However, the above ESI-MS spectra observed during the photolysis support an involvement of (**vi**) in the (**i**) → **1a** self-assembly, which implies that the Mo^V–Mo^V bond (with 2.6 Å) between the two Mo^V_3 triads is assisted by the condensation of $\{Mo^{VI}_1\}$ units with a resultant stabilization by hydrogen bonds between the Mo^V_3 triad μ_2-O atoms and the $Mo^{VI}O_3$ terminal O atoms (Figures 2 and 6).

Conclusion

Reddish-brown crystals of $[Me_3NH]_6[H_2Mo^V_{12}O_{28}(OH)_{12}(Mo^{VI}O_3)_4]\cdot 2H_2O$ (**1**), prepared by the long-term photolysis of PM-8 ($[^iPrNH_3]_6[Mo^{VI}_7O_{24}]\cdot 3H_2O$) in aqueous solutions,

inhibited the growth of human pancreatic cancer (AsPC-1) xenograft in the nude mice model and induced morphologic alteration in tumor.[6] The anion (**1a**) of **1**, a truncated tetrahedral ε-Keggin $\{Mo^{V}_{12}\}$ cluster capped by four $Mo^{VI}O_3$ units, involves twelve intramolecular hydrogen bonds between $Mo^{V}O_5(OH)$ μ_2-O and $Mo^{VI}O_3$ terminal O atoms, as was previously reported for $[Me_2NH_2]^+$ salt.[5] Spectrometries of ^{95}Mo NMR, electronic absorption, IR, and ESI-MS for aqueous solutions of **1a** indicate that the $\{\varepsilon$-$Mo^{V}_{12}\}$ core remains intact at pH 5–10 and that the detachment of the $Mo^{VI}O_3$ unit from **1a** proceeds at high pH level with an accompanying increase in the electronic transition of the Mo^{V}_2 pairs. Highly positive and negative potentials (0.8–0.9 V and -1.1–-1.2 V) of oxidation and reduction current peaks for the Mo^{V}_2 pairs of **1a** assist the structural stability of the ε-Keggin $\{Mo^{V}_{12}\}$ framework in aerobic solutions at pH 5–9. The processes of the photoreductive self-assembly from $[Mo^{VI}_7O_{24}]^{6-}$ (**i**) to **1a** are discussed with the help of structure of the species ($[(Mo^{VI}_6Mo^{V}O_{23})_2]^{10-}$) isolated during the short-term photolysis together with the solid-state photochemistry of PM-8, and schemes 4–9 are proposed based on an involvement of the formation of the half anion of **1a**, $[HMo^{V}_6O_{18}(OH)_6(Mo^{VI}O_3)_2]\}^{11-}$, which was supported by ESI-MS spectrometry of the photolytes. The proposed schemes support the formation of α-Keggin $\{Mo^{VI}_{12}\}$ species as a result of the condensation of four $[Mo^{VI}_3O_{13}]^{8-}$ moieties liberated during the photolysis of (**i**) to **1a**, which was previously implied.[7]

We acknowledge support from CREST of JST and Grants-in-Aid for Scientific Research No. 17002006 from the Ministry of Education, Culture, Sports, Science and Technology.

Supporting Information

Table S1 (Mo–O bond distances and inter-atomic distances for selected atoms), Table S2 (bond valence sums for all Mo and O atoms of Mo–O bonds), CIF (Crystallographic data for **1** with Cambridge Crystallographic Data Center depository number CCDC-626588), Figure S1 of cyclic voltammograms of **1** (0.2 mM) on glassy carbon electrode under aerobic conditions, and Figure S2 of ESI-MS spectra of the diluted samples for 11-mM PM-8 and the fully photolyzed (2-days photolysis) solutions at pH 5.5. These materials are available free of charge on the Web at: http://www.csj.jp/journals/bcsj/.

References

1 T. Yamase, *J. Mater. Chem.* **2005**, *15*, 4773.

2 a) T. Yamase, H. Fujita, K. Fukushima, *Inorg. Chim. Acta* **1988**, *151*, 15. b) T. Yamase, in *Polyoxometalates: From Platonic Solids to Anti-Retroviral Activity*, ed. by A. Müller, M. T. Pope, Kluwer Academic Publishers, Dordrecht, **1994**, p. 337.

3 T. Yamase, *J. Chem. Soc., Dalton Trans.* **1991**, 3055.

4 T. Yamase, P. Prokop, Y. Arai, *J. Mol. Struct.* **2003**, *656*, 107.

5 M. I. Khan, A. Müller, S. Dillinger, H. Bögge, Q. Chen, J. Zubieta, *Angew. Chem., Int. Ed. Engl.* **1993**, *32*, 1780.

6 A. Ogata, H. Yanagie, E. Ishikawa, Y. Morishita, S. Mitsui, A. Yamashita, K. Hasumi, S. Takamoto, T. Yamase, M. Eriguchi, *Br. J. Cancer* **2008**, *98*, 399.

7 T. Yamase, T. Ikawa, Y. Ohashi, Y. Sasada, *J. Chem. Soc., Chem. Commun.* **1979**, 697.

8 T. Yamase, T. Ikawa, *Bull. Chem. Soc. Jpn.* **1977**, *50*, 746.

9 $[PMo^{V}_8Mo^{VI}_4O_{36}(OH)_4\{La(H_2O)_4\}_4]Br_5\cdot 16H_2O$ was synthesized according to the reported literature,[10] and characterized by IR spectrometry.

10 P. Mialane, A. Dolbecq, L. Lisnard, A. Mallard, J. Marrot, F. Secheresse, *Angew. Chem., Int. Ed.* **2002**, *41*, 2398.

11 UV–vis spectrum of **1a** (0.2 mM) after the addition of increasing amounts of $Na_2MoO_4\cdot 2H_2O$ in the solution at pH 9–10 showed an increase of the absorption coefficient for the Mo^{V}_2 pairs and kept its intensity unchanged at least for 3 h at the ratio of initial concentration of $[Na_2MoO_4]/[\mathbf{1a}] = 20/1$.

12 T. Yamase, *Chem. Rev.* **1998**, *98*, 307.

13 a) T. Yamase, *J. Chem. Soc., Dalton Trans.* **1982**, 1987. b) T. Yamase, *Polyhedron* **1986**, *5*, 79. c) T. Yamase, M. Suga, *J. Chem. Soc., Dalton Trans.* **1989**, 661.

14 H. T. Evans, Jr., *Inorg. Chem.* **1966**, *6*, 967.

15 E. J. Graeber, B. Morosin, *Acta Crystallogr., Sect. B* **1977**, *33*, 2137.